Acta Mech 226, 3501–3519 (2015)
DOI 10.1007/s00707-015-1391-6

ORIGINAL PAPER

Dinh Gia Ninh · Dao Huy Bich · Bui Huy Kien

Torsional buckling and post-buckling behavior of eccentrically stiffened functionally graded toroidal shell segments surrounded by an elastic medium

Received: 4 March 2015 / Revised: 11 May 2015 / Published online: 19 June 2015

Abstract The nonlinear buckling and post-buckling problems of functionally graded stiffened toroidal shell segments surrounded by an elastic medium under torsion based on an analytical approach are investigated. The rings and stringers are attached to the shell, and material properties of the shell are assumed to be continuously graded in the thickness direction. The classical shell theory with the geometrical nonlinearity in von Kármán sense and the smeared stiffeners technique are applied to establish theoretical formulations. The three-term approximate solution of deflection is chosen more correctly, and the explicit expression to find critical load and post-buckling torsional load-deflection curves is given. The effects of geometrical parameters and the effectiveness of stiffeners on the stability of the shell are investigated.

1 Introduction

Functionally graded materials (FGMs) were known by Japanese scientists in 1984 [1]. This composite material is a mixture of ceramic and metallic constituent materials by continuously changing the volume fractions of their components. The advantage of FGMs is that they are better than the traditional fiber-reinforced and laminated composite materials in avoiding the stress concentration. FGMs are applied to heat-resistant, lightweight structures in aerospace, mechanical, and medical industries, etc. Therefore, the buckling and vibration problems of FGM structures have attracted much attention of researchers.

On the research of the torsional problem, Sofiyev et al. [2,3] pointed out the torsional vibration and buckling analysis of a cylindrical shell surrounded by an elastic medium. The torsion of a circular cylindrical bar made of either an isotropic compressible or an isotropic incompressible linear elastic material with material moduli varying only in the axial direction was taken into account by Batra [4]. The torsional post-buckling analysis of FGM cylindrical shells in thermal environment based on a higher-order shear deformation theory with a von Kármán–Donell type of kinematic nonlinearity was given by Shen [5]. Sofiyev and Schnack [6] presented the stability of a functionally graded cylindrical shell subjected to torsional loading varying as a linear function of time. The modified Donnell-type dynamic stability and compatibility equations were applied. The nonlinear buckling problem of FGM cylindrical shells under torsion load based on the nonlinear large deflection theory by using the energy method and the nonlinear strain–displacement relations of large deformation was studied by

D. G. Ninh (✉)
School of Mechanical Engineering, Hanoi University of Science and Technology, Hanoi, Vietnam
E-mail: ninhdinhgia@gmail.com; ninh.dinhgia@hust.edu.vn
Tel.: +84 988 287 789

D. H. Bich
Vietnam National University, Hanoi, Vietnam

B. H. Kien
Faculty of Mechanical Engineering, Hanoi University of Industry, Hanoi, Vietnam

Huang and Han [7]. Wang et al. [8] carried out the exact solutions and transient behavior for torsional vibration of functionally graded finite hollow cylinders. The torsional analysis of functionally graded hollow tubes of arbitrary shape based on governing equations in terms of Prandtl's stress function was investigated by Arghavan and Hematiyan [9]. Tan [10] developed the torsional buckling loads of thin and thick shells of revolution based on the classical thin shell theory and the first-order shear deformation shell theory. The nonlinear buckling and post-buckling problems of functionally graded stiffened thin circular cylindrical shells only subjected to torsional load by the analytical approach based on the classical shell theory with the geometrical nonlinearity in von Kármán sense were studied by Dung and Hoa [11]. The torsional stability analysis for thin cylindrical shells with the functionally graded middle layer resting on a Winkler elastic foundation was given by Sofiyev and Adiguzel [12]. The fundamental relations and basic equation of three-layered cylindrical shells with a FG middle layer resting on a Winkler elastic foundation under torsional load were derived. Zhang and Fu [13] addressed the torsional buckling characteristic of an elastic cylinder with a hard surface coating layer by Navier's equation and thin shell model. Recently, Dung and Hoa [14] investigated the nonlinear buckling and post-buckling of functionally graded stiffened thin circular cylindrical shells surrounded by an elastic foundation in thermal environments under torsional load by an analytical approach.

The nonlinear buckling and post-buckling of heat functionally graded cylindrical shells under combined axial compression and radial pressure were studied by Huang and Han [15]. Bich et al. [16] investigated the linear buckling of truncated conical panels made of functionally graded materials and subjected to axial compression, external pressure, and the combination of these loads. The nonlinear buckling behavior of truncated conical shells made of FGM using the large deformation theory with the von Kármán–Donnell type of kinematic nonlinearity subjected to a uniform axial compressive load was investigated by Sofiyev [17]. Furthermore, Duc et al. [18,19] presented an analytical approach to present the nonlinear static buckling and post-buckling for imperfect eccentrically stiffened FGM of shell structures on elastic foundations. The post-buckling analysis of axially loaded functionally graded cylindrical shells in thermal environments using the classical shell theory with von Kármán–Donnell type of kinematic nonlinearity was pointed out by Shen [20]. The dynamic buckling of imperfect FGM cylindrical shells with integrated surface-bonded sensor and actuator layers subjected to some complex combinations of thermo-electro-mechanical loads based on the general form of Green's strain tensor in curvilinear coordinates and a high-order shell theory proposed earlier was studied by Shariyat [21]. Liew et al. [22] calculated the post-buckling of FGM cylindrical shells under axial compression and thermal loads using the element-free kp-Ritz method. Kernel shape functions were used to approximate field variables and formulations based on the Ritz procedure which leads to a system of nonlinear discrete equations and overcomes the shortcomings of the conventional Rayleigh–Ritz method, in which it is difficult to choose appropriate global trial functions for problems with complicated boundary conditions. The linear thermal buckling and free vibration for functionally graded cylindrical shells subjected to a clamped–clamped boundary condition with temperature-dependent material properties were investigated by Kadoli and Ganesan [23]. The buckling behavior of FGM cylindrical shells subjected to pure bending load were taken into account by Huang et al. [24]. Sofiyev et al. [25] discussed the buckling of FGM hybrid truncated conical shells subjected to hydrostatic pressure. The author chose the available solution to satisfy the boundary condition, inserted them into the governing equations, and then used Galerkin's method to lead to pairs of time-dependent differential equations. Moreover, the thermal buckling of FGM sandwich plates was studied by Zenkour and Sobhy [26] using the sinusoidal shear deformation.

The shell on an elastic foundation has been studied by many authors. The simplest model for the elastic foundation is Winkler's model [27] like a series of separated springs without coupling effects between each other, and then a shear layer to one-parameter model is added by a Pasternak [28]. Bagherizadeh et al. [29] investigated the mechanical buckling of functionally graded material cylindrical shells surrounded by a Pasternak elastic foundation. Theoretical formulations were presented based on a higher-order shear deformation shell theory. Moreover, the post-buckling of FGM cylindrical shells surrounded by an elastic medium was presented by Shen [30,31]. Sofiyev [32,33] studied the buckling of FGM shells on an elastic foundation. The buckling of a heterogeneous orthotropic truncated conical shell under an axial load and surrounded by elastic media based on the finite deformation theory was investigated by Sofiyev [34]. The governing equations of elastic buckling of heterogeneous orthotropic truncated conical shells using von Kármán nonlinearity were given. Furthermore, Sofiyev [35] researched the nonlinear buckling of the FGM truncated conical shell surrounded by an elastic medium using the large deformation theory with von Kármán –Donnell type of kinematic nonlinearity.

Stein and McElman [36] carried out the buckling problem of homogenous and isotropic toroidal shell segments. Moreover, the initial post-buckling behavior of toroidal shell segments subject to several loading

conditions based on Koiter's general theory was performed by Hutchinson [37]. Parnell [38] gave a simple technique for the analysis of shells of revolution applied to toroidal shell segments.

To the best of the authors' knowledge, there has not been a study on the nonlinear torsional buckling of eccentrically stiffened FGM toroidal shell segments.

In the present paper, the nonlinear torsional buckling and post-buckling of eccentrically stiffened FGM toroidal shell segments surrounded by an elastic medium are investigated. Basing on the classical shell theory with nonlinear strain–displacement relation of large deflection, the Galerkin method is used for nonlinear buckling analysis of shells to give the expression of curves between deflection and torsional load. The effects of buckling modes, geometrical parameters, and volume fraction index on the nonlinear torsional buckling behavior of shells are investigated.

2 Governing equations

2.1 Functionally graded material (FGM)

Suppose that the material composition of the shell varies smoothly along the thickness in such a way that the inner surface is ceramic rich and the outer surface is metal rich by a simple power law in terms of the volume fractions of the constituents.

Denote V_{m} and V_{c} the volume fractions of metal and ceramic phases, respectively, which are related by $V_{\mathrm{m}} + V_{\mathrm{c}} = 1$ and V_{c} is expressed as $V_{\mathrm{m}}(z) = \left(\frac{2z+h}{2h}\right)^k$, where h is the thickness of the thin-walled structure, k is the volume-fraction exponent ($k \geq 0$); z is the thickness coordinate and varies from $-h/2$ to $h/2$; the subscripts m and c refer to the metal and ceramic constituents, respectively. According to the mentioned law, Young's modulus reads:

$$E(z) = E_{\mathrm{m}} V_{\mathrm{m}} + E_{\mathrm{m}} V_{\mathrm{m}} = E_{\mathrm{m}} + (E_{\mathrm{m}} - E_{\mathrm{m}}) \left(\frac{2z+h}{2h}\right)^k, \tag{1}$$

Poisson's ratio υ is assumed to be constant.

2.2 Constitutive relations and governing equations

Consider a functionally graded toroidal shell segment of thickness h and length L, which is formed by rotation of a plane circular arc of radius R about an axis in the plane of the curve as shown in Fig. 1. For the middle surface of a toroidal shell segment, from the figure:

$$r = a - R(1 - \sin\varphi),$$

where a is the equator radius and φ is the angle between the axis of revolution and the normal to the shell surface. For a sufficiently shallow toroidal shell in the region of the equator of the torus, the angle φ is approximately equal to $\pi/2$; thus, $\sin\varphi \approx 1$, $\cos\varphi \approx 0$, and $r = a$ [36]. The form of governing equation is simplified by putting:

$$\mathrm{d}x_1 = R\,\mathrm{d}\varphi, \quad dx_2 = a\,\mathrm{d}\theta.$$

The radius of arc R is positive with convex toroidal shell segment and negative with concave toroidal shell segment.

Suppose the FGM toroidal shell segment is reinforced by string and ring stiffeners. In order to provide continuity within the shell and stiffeners and easier manufacture, homogeneous stiffeners can be used. Because pure ceramic ones show brittleness, we used metal stiffeners and put them at the metal-rich side of the shell. With the law indicated in (1), the outer surface is metal rich, so the external metal stiffeners are put at the outer side of the shell.

The strains across the shell thickness at a distance z from the mid-surface are:

$$\varepsilon_1 = \varepsilon_1^0 - z\chi_1;\ \ \varepsilon_2 = \varepsilon_2^0 - z\chi_2;\ \ \gamma_{12} = \gamma_{12}^0 - 2z\chi_{12} \tag{2}$$

where ε_1^0 and ε_2^0 are normal strains, γ_{12}^0 is the shear strain at the middle surface of the shell, and χ_{ij} are the curvatures.

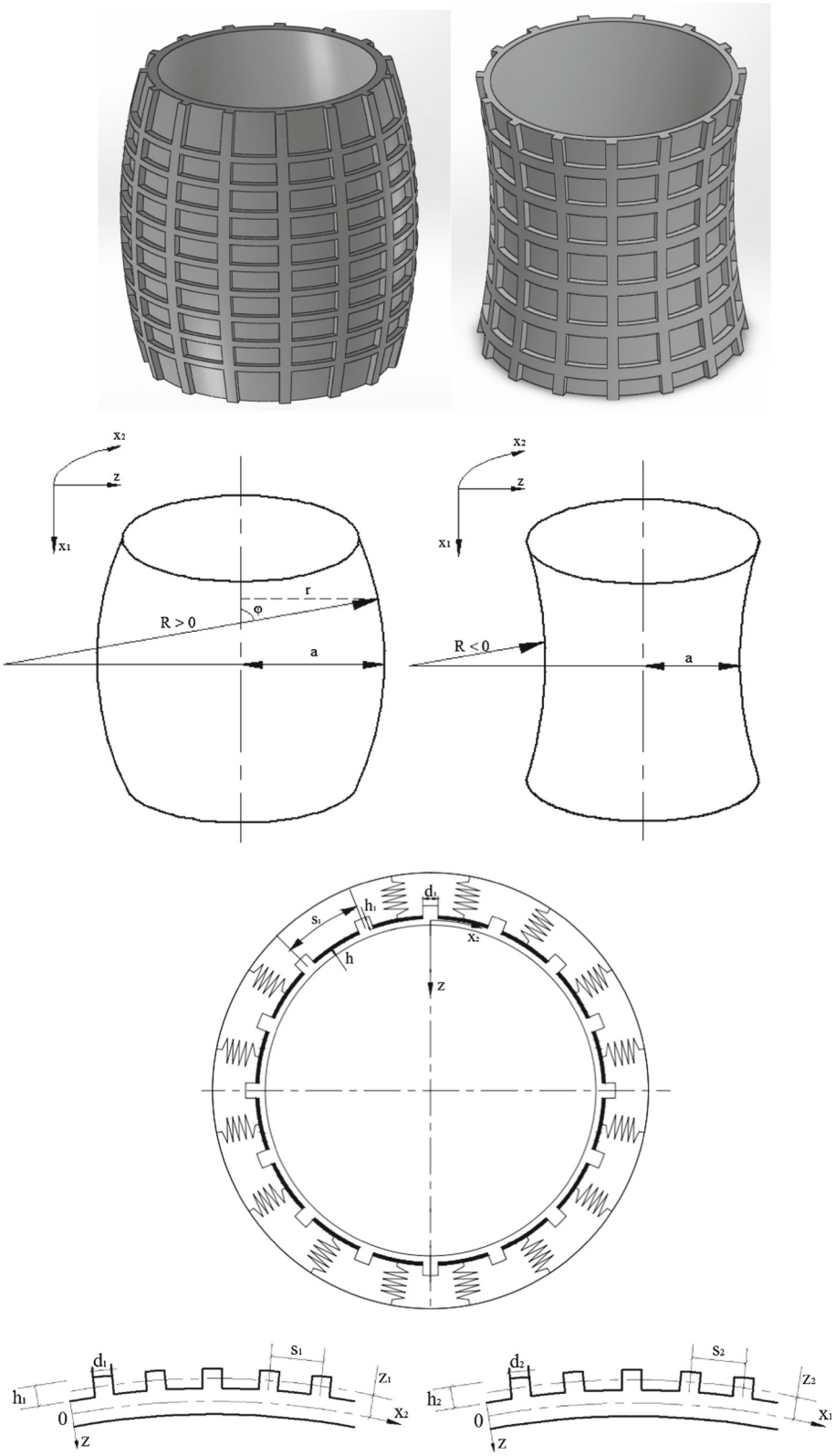

Fig. 1 Configuration of toroidal shell segments

According to the classical shell theory, the strains at the middle surface and curvatures are related to the displacement components u, v, w in the x_1, x_2, z coordinate directions as [39]:

$$\begin{aligned}
&\varepsilon_1^0 = \frac{\partial u}{\partial x_1} - \frac{w}{R} + \frac{1}{2}\left(\frac{\partial w}{\partial x_1}\right)^2; \quad \varepsilon_2^0 = \frac{\partial v}{\partial x_2} - \frac{w}{a} + \frac{1}{2}\left(\frac{\partial w}{\partial x_2}\right)^2; \\
&\gamma_{12}^0 = \frac{\partial u}{\partial x_2} + \frac{\partial v}{\partial x_1} + \frac{\partial w}{\partial x_1}\frac{\partial w}{\partial x_2}; \quad \chi_1 = \frac{\partial^2 w}{\partial x_1^2}; \ \chi_2 = \frac{\partial^2 w}{\partial x_2^2}; \ \chi_{12} = \frac{\partial^2 w}{\partial x_1 \partial x_2}.
\end{aligned} \tag{3}$$

From Eq. (3), the strains must be satisfied in the deformation compatibility equation

$$\frac{\partial^2 \varepsilon_1^0}{\partial x_2^2} + \frac{\partial^2 \varepsilon_2^0}{\partial x_1^2} - \frac{\partial^2 \gamma_{12}^0}{\partial x_1 \partial x_2} = -\frac{\partial^2 w}{R \partial x_2^2} - \frac{\partial^2 w}{a \partial x_1^2} + \left(\frac{\partial^2 w}{\partial x_1 \partial x_2}\right)^2 - \frac{\partial^2 w}{\partial x_1^2}\frac{\partial^2 w}{\partial x_2^2}. \tag{4}$$

Hooke's stress–strain relation is applied for the shell,

$$\begin{aligned}
\sigma_1^{sh} &= \frac{E(z)}{1-\nu^2}(\varepsilon_1 + \nu\varepsilon_2), \\
\sigma_2^{sh} &= \frac{E(z)}{1-\nu^2}(\varepsilon_2 + \nu\varepsilon_1), \\
\sigma_{12}^{sh} &= \frac{E(z)}{2(1+\nu)}\gamma_{12}.
\end{aligned} \tag{5}$$

And for metal stiffeners

$$\begin{aligned}
\sigma_1^{st} &= E_{\mathrm{m}}\varepsilon_1, \\
\sigma_2^{st} &= E_{\mathrm{m}}\varepsilon_2.
\end{aligned} \tag{6}$$

Taking into account the contribution of stiffeners by the smeared stiffeners technique and omitting the twist of stiffeners and integrating the stress–strain equations and their moments through the thickness of the shell, we obtain the expressions for force and moment resultants of ES-FGM toroidal shell segment:

$$\begin{aligned}
N_1 &= \left(A_{11} + \frac{E_{\mathrm{m}}A_1}{s_1}\right)\varepsilon_1^0 + A_{12}\varepsilon_2^0 - (B_{11} + C_1)\chi_1 - B_{12}\chi_2, \\
N_2 &= A_{12}\varepsilon_1^0 + \left(A_{22} + \frac{E_{\mathrm{m}}A_2}{s_2}\right)\varepsilon_2^0 - B_{12}\chi_1 - (B_{22} + C_2)\chi_2, \\
N_{12} &= A_{66}\gamma_{12}^0 - 2B_{66}\chi_{12},
\end{aligned} \tag{7}$$

$$\begin{aligned}
M_1 &= (B_{11} + C_1)\varepsilon_1^0 + B_{12}\varepsilon_2^0 - \left(D_{11} + \frac{E_{\mathrm{m}}I_1}{s_1}\right)\chi_1 - D_{12}\chi_2, \\
M_2 &= B_{12}\varepsilon_1^0 + (B_{22} + C_2)\varepsilon_2^0 - D_{12}\chi_1 - \left(D_{22} + \frac{E_{\mathrm{m}}I_2}{s_2}\right)\chi_2, \\
M_{12} &= B_{66}\gamma_{12}^0 - 2D_{66}\chi_{12}
\end{aligned} \tag{8}$$

where A_{ij}, B_{ij}, D_{ij} $(i, j = 1, 2, 6)$ are extensional, coupling, and bending stiffnesses of the shell without stiffeners.

$$\begin{aligned}
&A_{11} = A_{22} = \frac{E_1}{1-\nu^2}, \quad A_{12} = \frac{E_1.\nu}{1-\nu^2}, \quad A_{66} = \frac{E_1}{2(1+\nu)}, \\
&B_{11} = B_{22} = \frac{E_2}{1-\nu^2}, \quad B_{12} = \frac{E_2.\nu}{1-\nu^2}, \quad B_{66} = \frac{E_2}{2(1+\nu)}, \\
&D_{11} = D_{22} = \frac{E_3}{1-\nu^2}, \quad D_{12} = \frac{E_3.\nu}{1-\nu^2}, \quad D_{66} = \frac{E_3}{2(1+\nu)},
\end{aligned} \tag{9}$$

and

$$\begin{aligned} E_1 &= \left(E_{\mathrm{m}} + \frac{E_{\mathrm{m}} - E_{\mathrm{m}}}{k+1}\right)h, \quad E_2 = \frac{(E_{\mathrm{m}} - E_{\mathrm{m}})kh^2}{2(k+1)(k+2)}, \\ E_3 &= \left[\frac{E_{\mathrm{m}}}{12} + (E_{\mathrm{m}} - E_{\mathrm{m}})\left(\frac{1}{k+3} - \frac{1}{k+2} + \frac{1}{4k+4}\right)\right]h^3, \end{aligned} \tag{10}$$

and

$$\begin{aligned} C_1 &= \pm\frac{E_{\mathrm{m}}A_1 z_1}{s_1}, \quad C_2 = \pm\frac{E_{\mathrm{m}}A_2 z_2}{s_2}, \\ A_1 &= h_1 d_1, \ A_2 = h_2 d_2, \\ I_1 &= \frac{d_1 h_1^3}{12} + A_1 z_1^2, \quad I_2 = \frac{d_2 h_2^3}{12} + A_2 z_2^2. \end{aligned} \tag{11}$$

In the above relations (7), (8), (10), and (11), E_{m} is the elasticity modulus of the metal stiffener which is assumed to be identical for both types of stiffeners. The spacings of the stringer and ring stiffeners are denoted by s_1 and s_2, respectively. The quantities A_1, A_2 are the cross section areas of the stiffeners, and I_1, I_2, z_1, z_2 are the second moments of cross section areas and eccentricities of the stiffeners with respect to the middle surface of the shell, respectively. The sign minus of C_1 and C_2 depends on external stiffeners.

Remark Conversely, if the inner side of FGM shell is metal rich with existence of metal stiffeners, all calculated expressions can be used, but one must replace E_{c} and E_{m} each to other in Eq. (10), and the plus sign is taken in Eq. (11).

The nonlinear equilibrium equations of a toroidal shell segment surrounded by an elastic foundation based on the classical shell theory are given by [39]:

$$\frac{\partial N_1}{\partial x_1} + \frac{\partial N_{12}}{\partial x_2} = 0, \tag{12.1}$$

$$\frac{\partial N_{12}}{\partial x_1} + \frac{\partial N_2}{\partial x_2} = 0, \tag{12.2}$$

$$\frac{\partial^2 M_1}{\partial x_1^2} + 2\frac{\partial^2 M_{12}}{\partial x_1 \partial x_2} + \frac{\partial^2 M_2}{\partial x_2^2} + N_1\frac{\partial^2 w}{\partial x_1^2} + 2N_{12}\frac{\partial^2 w}{\partial x \partial y} \tag{12.3}$$

$$+ N_2\frac{\partial^2 w}{\partial x_2^2} + \frac{N_1}{R} + \frac{N_2}{a} - K_1 w + K_2\left(\frac{\partial^2 w}{\partial x_1^2} + \frac{\partial^2 w}{\partial x_2^2}\right) = 0 \tag{12.4}$$

where K_1 (N/m^3) is the linear stiffness of the foundation and K_2(N/m) is the shear modulus of the subgrade.

Considering the first two of Eqs. (12), a stress function may be defined as:

$$N_1^1 = \frac{\partial^2 F}{\partial x_2^2}, \quad N_2^1 = \frac{\partial^2 F}{\partial x_1^2}, \quad N_{12}^1 = -\frac{\partial^2 F}{\partial x_1 \partial x_2}. \tag{13}$$

The reverse relations are obtained from Eq. (7)

$$\begin{aligned} \varepsilon_1^0 &= A_{22}^* N_1 - A_{12}^* N_2 + B_{11}^* \chi_1 + B_{12}^* \chi_2, \\ \varepsilon_2^0 &= A_{11}^* N_2 - A_{12}^* N_1 + B_{21}^* \chi_1 + B_{22}^* \chi_2, \\ \gamma_{12}^0 &= A_{66}^* N_{12} + 2B_{66}^* \chi_{12}, \end{aligned} \tag{14}$$

where

$$\begin{aligned} A_{11}^* &= \frac{1}{\Delta}\left(A_{11} + \frac{E_0 A_1}{s_1}\right), \quad A_{22}^* = \frac{1}{\Delta}\left(A_{22} + \frac{E_0 A_2}{s_2}\right), \quad A_{12}^* = \frac{A_{12}}{\Delta}, \quad A_{66}^* = \frac{1}{A_{66}}, \\ \Delta &= \left(A_{11} + \frac{E_0 A_1}{s_1}\right).\left(A_{22} + \frac{E_0 A_2}{s_2}\right) - A_{12}^2; \\ B_{11}^* &= A_{22}^*(B_{11} + C_1) - A_{12}^* B_{12}, \quad B_{22}^* = A_{11}^*(B_{22} + C_2) - A_{12}^* B_{12}, \\ B_{12}^* &= A_{22}^* B_{12} - A_{12}^*(B_{22} + C_2), \quad B_{21}^* = A_{11}^*.B_{12} - A_{12}^*(B_{11} + C_1), \quad B_{66}^* = \frac{B_{66}}{A_{66}}. \end{aligned}$$

Substituting Eq. (14) in Eq. (8) yields

$$\begin{aligned} M_1 &= B_{11}^* N_1 + B_{21}^* N_2 - D_{11}^* \chi_1 - D_{12}^* \chi_2, \\ M_2 &= B_{12}^* N_1 + B_{22}^* N_2 - D_{21}^* \chi_1 - D_{22}^* \chi_2, \\ M_{12} &= B_{66}^* N_{12} - 2D_{66}^* \chi_{12} \end{aligned} \tag{15}$$

where

$$\begin{aligned} D_{11}^* &= D_{11} + \frac{E_0 I_1}{s_1} - (B_{11} + C_1) B_{11}^* - B_{12} B_{21}^*, \\ D_{22}^* &= D_{22} + \frac{E_0 I_2}{s_2} - B_{12} B_{21}^* - (B_{22} + C_2) B_{22}^*, \\ D_{12}^* &= D_{12} - (B_{11} + C_1) B_{12}^* - B_{12} B_{22}^*, \\ D_{21}^* &= D_{12} - B_{12} B_{11}^* - (B_{22} + C_2) B_{21}^*, \\ D_{66}^* &= D_{66} - B_{66} B_{66}^*. \end{aligned}$$

The substitution of Eq. (14) in the compatibility Eqs. (4) and (15) in Eq. (12.3), taking into account expressions (3) and (13), yields a system of equations

$$\begin{aligned} &A_{11}^* \frac{\partial^4 F}{\partial x_1^4} + (A_{66}^* - 2A_{12}^*) \frac{\partial^4 F}{\partial x_1^2 \partial x_2^2} + A_{22}^* \frac{\partial^4 F}{\partial x_2^4} + B_{21}^* \frac{\partial^4 w}{\partial x_1^4} + (B_{11}^* + B_{22}^* - 2B_{66}^*) \frac{\partial^4 w}{\partial x_1^2 \partial x_2^2} + \\ &+ B_{12}^* \frac{\partial^4 w}{\partial x_2^4} = -\frac{1}{R} \frac{\partial^2 w}{\partial x_2^2} - \frac{1}{a} \frac{\partial^2 w}{\partial x_1^2} + \left(\frac{\partial^2 w}{\partial x_1 \partial x_2} \right)^2 - \frac{\partial^2 w}{\partial x_1^2} \frac{\partial^2 w}{\partial x_2^2}, \end{aligned} \tag{16}$$

$$\begin{aligned} &B_{21}^* \frac{\partial^4 F}{\partial x_1^4} + (B_{11}^* + B_{22}^* - 2B_{66}^*) \frac{\partial^4 F}{\partial x_1^2 \partial x_2^2} + B_{12}^* \frac{\partial^4 F}{\partial x_2^4} - D_{11}^* \frac{\partial^4 w}{\partial x_1^4} - (D_{12}^* + D_{21}^* + 4D_{66}^*) \frac{\partial^4 w}{\partial x_1^2 \partial x_2^2} \\ &- D_{22}^* \frac{\partial^4 w}{\partial x_2^4} + \frac{1}{R} \frac{\partial^2 F}{\partial x_2^2} + \frac{1}{a} \frac{\partial^2 F}{\partial x_1^2} + \frac{\partial^2 F}{\partial x_2^2} \frac{\partial^2 w}{\partial x_1^2} - 2 \frac{\partial^2 F}{\partial x_1 \partial x_2} \frac{\partial^2 w}{\partial x_1 \partial x_2} + \frac{\partial^2 F}{\partial x_1^2} \frac{\partial^2 w}{\partial x_2^2} - K_1 w \\ &+ K_2 \left(\frac{\partial^2 w}{\partial x_1^2} + \frac{\partial^2 w}{\partial x_2^2} \right) = 0. \end{aligned} \tag{17}$$

3 Nonlinear torsional buckling analysis

The FGM toroidal shell segment is assumed to be simply supported at its edges $x_1 = 0$ and $x_1 = L$ and subjected to torsional load on the circular base of the shell.

The edge is simply supported and freely movable (FM) in the axial direction. The associated boundary conditions are:

$$w = 0, \quad M_1 = 0, \quad N_1 = 0, \quad N_{12} = \tau h \text{ at } x_1 = 0;\ L. \tag{18}$$

With the consideration of boundary conditions (18), the deflection of the shell in this case can be expressed by [7]:

$$w = W_0 + W_1 \sin \gamma_m x_1 \sin \beta_n (x_2 - \lambda x_1) + W_2 \sin^2 \gamma_m x_1, \tag{19}$$

in which $\gamma_m = \frac{m\pi}{L}$, $\beta_n = \frac{n}{a}$, and m, n are the half wave numbers along x_1-axis and wave numbers along x_2-axis, respectively. The first term of w in Eq. (19) represents the uniform deflection of points belonging to two butt ends $x_1 = 0$ and $x_1 = L$, the second term—a linear buckling shape, and the third—a nonlinear buckling shape.

As can be seen, the simply supported boundary condition at $x_1 = 0$ and $x_1 = L$ is fulfilled in the average sense.

Substituting Eq. (19) in Eq. (16) one obtains

$$A_{11}^{*}\frac{\partial^4 F}{\partial x_1^4}+(A_{66}^{*}-2A_{12}^{*})\frac{\partial^4 F}{\partial x_1^2\partial x_2^2}+A_{22}^{*}\frac{\partial^4 F}{\partial x_2^4}=H_{01}\cos 2\gamma_m x_1+H_{02}\cos 2\beta_n(x_2-\lambda x_1)$$
$$+H_{03}\left\{\cos\beta_n\left[x_2-\left(\frac{3\gamma_m}{\beta_n}+\lambda\right)x_1\right]-\cos\beta_n\left[x_2+\left(\frac{3\gamma_m}{\beta_n}-\lambda\right)x_1\right]\right\}$$
$$+H_{04}\cos\beta_n\left[x_2-\left(\frac{\gamma_m}{\beta_n}+\lambda\right)x_1\right]+H_{05}\cos\beta_n\left[x_2+\left(\frac{\gamma_m}{\beta_n}-\lambda\right)x_1\right] \tag{20}$$

where

$$H_{01}=\left[2\gamma_m^2\left(4B_{21}^{*}\gamma_m^2-\frac{1}{a}\right)\right]W_2+\frac{1}{2}W_1^2\gamma_m^2\beta_n^2;\quad H_{02}=\frac{1}{2}\gamma_m^2\beta_n^2W_1^2;\quad H_{03}=\frac{1}{2}\gamma_m^2\beta_n^2W_1W_2;$$
$$H_{04}=\frac{1}{2}W_1\left\{-B_{21}^{*}(\gamma_m^2+\beta_n^2\lambda^2)^2+(2\gamma_m\beta_n\lambda)^2+\left[\frac{1}{a}-\beta_n^2(B_{11}^{*}+B_{22}^{*}-2B_{66}^{*})\right](\gamma_m^2+\beta_n^2\lambda^2)-B_{12}^{*}\beta_n^4\right.$$
$$\left.+2\gamma_m\beta_n\lambda\left[-2B_{21}^{*}(\gamma_m^2+\beta_n^2\lambda^2)+\frac{1}{a}-(B_{11}^{*}+B_{22}^{*}-2B_{66}^{*})\beta_n^2\right]\right\}-\frac{1}{2}\gamma_m^2\beta_n^2W_1W_2+\frac{1}{2R}\beta_n^2W_1;$$
$$H_{05}=W_1\left\{\frac{1}{2}B_{21}^{*}\left[(\gamma_m^2+\beta_n^2\lambda^2)^2+(2\gamma_m\beta_n\lambda)^2\right]-\frac{1}{2}\left[\frac{1}{a}-\beta_n^2(B_{11}^{*}+B_{22}^{*}-2B_{66}^{*})\right](\gamma_m^2+\beta_n^2\lambda^2)+B_{12}^{*}\gamma_n^4\right.$$
$$\left.+\gamma_m\beta_n\lambda\left[-2B_{21}^{*}(\gamma_m^2+\beta_n^2\lambda^2)+\frac{1}{a}-(B_{11}^{*}+B_{22}^{*}-2B_{66}^{*})\beta_n^2\right]\right\}+\frac{1}{2}\gamma_m^2\beta_n^2W_1W_2-\frac{1}{2R}\beta_n^2W_1. \tag{21}$$

The general solution of Eq. (20) for a torsion-loaded shell is of the form

$$F=H_1\cos 2\gamma_m x_1+H_2\cos 2\beta_n(x_2-\lambda x_1)$$
$$+H_3\cos\beta_n\left[x_2-\left(\frac{3\gamma_m}{\beta_n}+\lambda\right)x_1\right]+H_4\cos\beta_n\left[x_2+\left(\frac{3\gamma_m}{\beta_n}-\lambda\right)x_1\right]$$
$$+H_5\cos\beta_n\left[x_2-\left(\frac{\gamma_m}{\beta_n}+\lambda\right)x_1\right]+H_6\cos\beta_n\left[x_2+\left(\frac{\gamma_m}{\beta_n}-\lambda\right)x_1\right]-\tau h x_1x_2 \tag{22}$$

where τ is the torsional load intensity and the coefficients H_i $(i=1\div 8)$ are defined by:

$$H_1=\frac{H_{01}}{16\gamma_m^4A_{11}^{*}}=M_1W_2+M_2W_1^2;$$
$$H_2=\frac{H_{02}}{16\beta_n^4[A_{11}^{*}\lambda^4+(A_{66}^{*}-2A_{12}^{*})\lambda^2+A_{22}^{*}]}=M_3W_1^2;$$
$$H_3=\frac{H_{03}}{\beta_n^4\left[A_{11}^{*}\left(\frac{3\gamma_m}{\beta_n}+\lambda\right)^4+(A_{66}^{*}-2A_{12}^{*})\left(\frac{3\gamma_m}{\beta_n}+\lambda\right)^2+A_{22}^{*}\right]}=M_4W_1W_2;$$
$$H_4=\frac{-H_{03}}{\beta_n^4\left[A_{11}^{*}\left(\frac{3\gamma_m}{\beta_n}-\lambda\right)^4+(A_{66}^{*}-2A_{12}^{*})\left(\frac{3\gamma_m}{\beta_n}-\lambda\right)^2+A_{22}^{*}\right]}=M_5W_1W_2;$$
$$H_5=\frac{H_{04}}{\beta_n^4\left[A_{11}^{*}\left(\frac{\gamma_m}{\beta_n}+\lambda\right)^4+(A_{66}^{*}-2A_{12}^{*})\left(\frac{\gamma_m}{\beta_n}+\lambda\right)^2+A_{22}^{*}\right]}=M_6W_1+M_7W_1W_2;$$
$$H_6=\frac{H_{05}}{\beta_n^4\left[A_{11}^{*}\left(\frac{\gamma_m}{\beta_n}-\lambda\right)^4+(A_{66}^{*}-2A_{12}^{*})\left(\frac{\gamma_m}{\beta_n}-\lambda\right)^2+A_{22}^{*}\right]}=M_8W_1+M_9W_1W_2 \tag{23}$$

in which

$$M_1 = \frac{4B_{21}^*\gamma_m^2 - \frac{1}{a}}{8\gamma_m^2 A_{11}^*};\quad M_2 = \frac{\beta_n^2}{32\gamma_m^2 A_{11}^*};\quad M_3 = \frac{\gamma_m^2}{32\beta_n^2[A_{11}^*\lambda^4 + (A_{66}^* - 2A_{12}^*)\lambda^2 + A_{22}^*]};$$

$$M_4 = \frac{\gamma_m^2}{\beta_n^2\left[A_{11}^*\left(\frac{3\gamma_m}{\beta_n} + \lambda\right)^4 + (A_{66}^* - 2A_{12}^*)\left(\frac{3\gamma_m}{\beta_n} + \lambda\right)^2 + A_{22}^*\right]};$$

$$M_5 = \frac{-\gamma_m^2}{\beta_n^2\left[A_{11}^*\left(\frac{3\gamma_m}{\beta_n} - \lambda\right)^4 + (A_{66}^* - 2A_{12}^*)\left(\frac{3\gamma_m}{\beta_n} - \lambda\right)^2 + A_{22}^*\right]};$$

$$M_6 = \frac{\begin{array}{l}\frac{1}{2}\Big\{-B_{21}^*(\gamma_m^2 + \beta_n^2\lambda^2)^2 + (2\gamma_m\beta_n\lambda)^2 + \left[\frac{1}{a} - \beta_n^2(B_{11}^* + B_{22}^* - 2B_{66}^*)\right](\gamma_m^2 + \beta_n^2\lambda^2) - B_{12}^*\beta_n^4 \\ \quad + 2\gamma_m\beta_n\lambda\left[-2B_{21}^*(\gamma_m^2 + \beta_n^2\lambda^2) + \frac{1}{a} - (B_{11}^* + B_{22}^* - 2B_{66}^*)\beta_n^2\right]\Big\} + \frac{1}{2R}\beta_n^2\end{array}}{\beta_n^4\left[A_{11}^*\left(\frac{\gamma_m}{\beta_n} + \lambda\right)^4 + (A_{66}^* - 2A_{12}^*)\left(\frac{\gamma_m}{\beta_n} + \lambda\right)^2 + A_{22}^*\right]};$$

$$M_7 = \frac{-\frac{1}{2}\gamma_m^2}{\beta_n^2\left[A_{11}^*\left(\frac{\gamma_m}{\beta_n} + \lambda\right)^4 + (A_{66}^* - 2A_{12}^*)\left(\frac{\gamma_m}{\beta_n} + \lambda\right)^2 + A_{22}^*\right]};$$

$$M_8 = \frac{\begin{array}{l}\Big\{\frac{1}{2}B_{21}^*\left[(\gamma_m^2 + \beta_n^2\lambda^2)^2 + (2\gamma_m\beta_n\lambda)^2\right] - \frac{1}{2}\left[\frac{1}{a} - \beta_n^2(B_{11}^* + B_{22}^* - 2B_{66}^*)\right](\gamma_m^2 + \beta_n^2\lambda^2) + B_{12}^*\gamma_n^4 \\ \quad + \gamma_m\beta_n\lambda\left[-2B_{21}^*(\gamma_m^2 + \beta_n^2\lambda^2) + \frac{1}{a} - (B_{11}^* + B_{22}^* - 2B_{66}^*)\beta_n^2\right]\Big\} - \frac{1}{2R}\beta_n^2\end{array}}{\beta_n^4\left[A_{11}^*\left(\frac{\gamma_m}{\beta_n} - \lambda\right)^4 + (A_{66}^* - 2A_{12}^*)\left(\frac{\gamma_m}{\beta_n} - \lambda\right)^2 + A_{22}^*\right]};$$

$$M_9 = \frac{\frac{1}{2}\gamma_m^2}{\beta_n^2\left[A_{11}^*\left(\frac{\gamma_m}{\beta_n} - \lambda\right)^4 + (A_{66}^* - 2A_{12}^*)\left(\frac{\gamma_m}{\beta_n} - \lambda\right)^2 + A_{22}^*\right]}. \tag{24}$$

Equation (17) will be evaluated by the Galerkin method. The procedure is performed in the following:

Substituting Eqs. (19) and (22) in the left side of Eq. (17), then multiplying the obtained equation in turn with each shape function of Eq. (19), and integrating in the ranges $0 \le x_1 \le L;\ 0 \le x_2 \le 2\pi a$ and after some calculations lead to:

$$S_1 + S_2 W_2 + S_3 W_1^2 + S_4 W_2^2 + 2\tau\beta^2\lambda h = 0, \tag{25}$$

$$S_5 W_2 + S_6 W_1^2 + S_7 W_1^2 W_2 + 2K_1 W_0 = 0 \tag{26}$$

where

$$\begin{aligned} S_1 = \Bigg\{ & \left[B_{21}^*(\gamma_m + \beta_n\lambda)^4 + B_{12}^*\beta_n^4 + \beta_n^2(B_{11}^* + B_{22}^* - 2B_{66}^*)(\gamma_m + \beta_n\lambda)^2 - \frac{\beta_n^2}{R} - \frac{(\gamma_m + \beta_n\lambda)^2}{a}\right] M_6 \\ & - \left[B_{21}^*(\gamma_m - \beta_n\lambda)^4 + B_{12}^*\beta_n^4 + \beta_n^2(B_{11}^* + B_{22}^* - 2B_{66}^*)(\gamma_m - \beta_n\lambda)^2 - \frac{\beta_n^2}{R} - \frac{(\gamma_m - \beta_n\lambda)^2}{a}\right] M_8 \\ & - \frac{D_{11}^*}{2}\left[(\gamma_m + \beta_n\lambda)^4 + (\gamma_m - \beta_n\lambda)^4\right] \\ & - (D_{12}^* + D_{21}^* + 4D_{66}^*)\beta_n^3\gamma_m\lambda - D_{22}^*\beta_n^4 - K_1 - K_2\left(\gamma_m^2 + \beta_n^2\lambda^2\right) - K_2\beta_n^2 \Bigg\}, \end{aligned}$$

$$
\begin{aligned}
S_2 = &\left\{\left[B_{21}^*(\gamma_m+\beta_n\lambda)^4 + B_{12}^*\beta_n^4 + \beta_n^2(B_{11}^*+B_{22}^*-2B_{66}^*)(\gamma_m+\beta_n\lambda)^2 - \frac{\beta_n^2}{R} - \frac{(\gamma_m+\beta_n\lambda)^2}{a}\right] M_7\right.\\
&-\left[B_{21}^*(\gamma_m-\beta_n\lambda)^4 + B_{12}^*\beta_n^4 + \beta_n^2(B_{11}^*+B_{22}^*-2B_{66}^*)(\gamma_m-\beta_n\lambda)^2 - \frac{\beta_n^2}{R} - \frac{(\gamma_m-\beta_n\lambda)^2}{a}\right] M_9\\
&\left.+(M_6-M_8)\,\gamma_m^2\beta_n^2 - 2M_1\gamma_m^2\beta_n^2\right\},\\
S_3 = &-2\left[M_3\beta_n^2\left(\gamma_m^2+\beta_n^2\lambda^2\right) - 2M_3\beta_n^4\lambda^2 + M_2\gamma_m^2\beta_n^2 + M_3\beta_n^4\lambda^2\right],\\
S_4 = &\,\gamma_m^2\beta_n^2\,(M_5+M_7-M_4-M_9)\,,\\
S_5 = &\left[\left(16B_{21}^*\gamma_m^4 - \frac{4\gamma_m^2}{a}\right)M_1 + 8\gamma_m^4 D_{11}^* + \frac{3K_1}{2} + 2K_2\gamma_m^2\right],\\
S_6 = &\left[\left(16B_{21}^*\gamma_m^4 - \frac{4\gamma_m^2}{a}\right)M_2 + M_8\beta_n^2(\gamma_m^2+\beta_n^2\lambda^2-\gamma_m^2\beta_n^2\lambda^2) - M_6\beta_n^2(\gamma_m^2+\beta_n^2\lambda^2-\gamma_m^2\beta_n^2\lambda^2)\right],\\
S_7 = &\,\gamma_m^2\beta_n^2\,(M_4+M_9-M_5-M_7)\,.
\end{aligned}
\tag{27}
$$

Furthermore, the toroidal shell segments have to also satisfy the circumferential closed condition [7,15] as:

$$
\int_0^L\int_0^{2\pi a}\frac{\partial v}{\partial x_2}dx_1dx_2 = \int_0^L\int_0^{2\pi a}\left[\varepsilon_2^0 + \frac{w}{a} - \frac{1}{2}\left(\frac{\partial w}{\partial x_2}\right)^2\right]\mathrm{d}x_1\mathrm{d}x_2 = 0. \tag{28}
$$

Using Eqs. (13), (14), and (19), the integral becomes:

$$
8W_0 + 4W_2 - W_1^2 a\beta_n^2 = 0. \tag{29}
$$

Substituting W_0 in Eqs. (26)–(29), then substituting W_1^2 in Eq. (26) into Eq. (25) leads to an equation representing the $\tau \sim W_2$ relation as

$$
\tau = -\left(S_1 + W_2S_2 + \frac{K_1 - S_5}{S_6 + S_7W_2 + \frac{K_1a\beta_n^2}{4}}S_3W_2 + W_2^2S_4\right)\frac{1}{2\beta_n^2\lambda h}. \tag{30}
$$

Equation (30) expresses the post-buckling $\tau \sim W_2$ curves of stiffened FGM toroidal shell segments. When $W_2 \to 0$, Eq. (30) becomes

$$
\tau = -\frac{S_1}{2\beta_n^2\lambda h}. \tag{31}
$$

Equation (31) is used to show upper critical loads in case of a linear buckling shape.

From Eq. (19), it can be seen that the maximal deflection of the shells

$$
w_{\max} = W_0 + W_1 + W_2 \tag{32}
$$

locates at $x_1 = iL/(2m)$, $x_2 = j\pi a/(2n) + i\lambda L/(2m)$, where i and j are odd integer numbers.

Solving W_1 and W_0 from Eqs. (25), (26), and (29) with respect to W_2 and then substituting them in Eq. (32) leads to

$$
W_{\max} = \frac{a\beta_n^2}{8}\left(\frac{K_1W_2 - S_5W_2}{S_6 + S_7W_2 + \frac{K_1a\beta_n^2}{4}}\right) + \sqrt{\frac{K_1W_2 - S_5W_2}{S_6 + S_7W_2 + \frac{K_1a\beta_n^2}{4}}} + \frac{W_2}{2}. \tag{33}
$$

Combining Eq. (30) with Eq. (33), the post-buckling load-maximal deflection curves of stiffened FGM toroidal shell segments can be derived.

Table 1 Comparisons of critical torsional load τ (psi) for an un-stiffened isotropic cylindrical shell

τ (psi)	Exp of Nash [40]	Shen [5]	Present ($\lambda = 0.23$)	Error (%)
$E = 27e6$ psi, $\nu = 0.3$; $L = 38$ in, $R = 4$ in, $h = 0.0172$ in	6590	6835 $(m, n) = (1, 2)$	6712.767 $(m, n) = (1, 3)$	1.86 (exp) 1.79 (Shen)

Table 2 Comparisons of critical torsional load τ (psi) for an un-stiffened isotropic cylindrical shell

τ (psi)	Exp of Ekstrom [41]	Shen [5]	Present ($\lambda = 0.1$)	Error (%)
$E = 29e6$ psi, $\nu = 0.3$; $L = 19.85$ in, $R = 3$ in, $h = 0.0075$ in	4800	4997 $(m, n) = (1, 3)$	4968.131 $(m, n) = (1, 3)$	3.50 (exp) 0.58 (Shen)

Table 3 Comparisons of critical torsional load τ (MPa) for an FGM cylindrical shell

	R/h	$L/R = 1$	$L/R = 1.5$	$L/R = 2$
Huang and Han	400	48.90 (15, 0.39)	39.25 (13, 0.33)	33.82 (12, 0.31)
Present		48.40 (15, 0.41)	39.67 (13, 0.29)	33.96 (12, 0.24)
Huang and Han	500	36.78 (16, 0.36)	29.61 (14, 0.32)	25.58 (13, 0.30)
Present		36.27 (16, 0.36)	29.91 (14, 0.26)	25.30 (13, 0.22)

4 Results and discussion

4.1 Validation of the present study

Up to now, there is no publication about an FGM toroidal shell segment under torsional load, which is the reason to compare the post-buckling path of the FGM cylindrical shell (i.e., a toroidal shell segment with $R \to \infty$). Two comparisons on the critical load are given to validate the present study.

Firstly, the present results will be compared with the results for an un-stiffened isotropic cylindrical shell under torsion load given by Shen [5] using the higher-order shear deformation shell theory and the experimental results of Nash [40] and Ekstrom [41]. In Tables 1 and 2, the critical torsional loads τ are calculated by Eqs. (30) for an un-stiffened isotropic shell without an elastic foundation and where the material of the shell is full of metal.

Tables 1 and 2 show good agreements in these comparisons.

Secondly, the torsional post-buckling behavior of an FGM cylindrical shell in the present paper is analyzed by the Galerkin method. The obtained results are compared with the results of Huang and Han [7] who used the other method—Ritz method. Equations (30) and (33) are used to determine the critical loads of an FGM cylindrical shell without an elastic foundation. An FGM cylindrical shell is made of ZrO_2/ Ti-6Al-4V material at initial temperature $T_0 = 300K$ by considering the following material properties of torsional load (Table 3):

$$E_c = 168.0421\text{GPa};\ E_m = 105.6835GPa\text{GPa};\ \upsilon = 0.3;\ k = 1.$$

4.2 Results of nonlinear torsional buckling of FGM toroidal shell segments

To illustrate the proposed approach, we consider ceramic–metal functionally graded toroidal shell segments that consist of aluminum and alumina with the following properties: $E_m = 70 \times 10^9$ N/m^2; $E_m = 380 \times 10^9$ N/m^2 (whereas Poisson's ratio is chosen to be 0.3).

4.2.1 Effect of the mode (m, n, λ) on the critical torsional load

The geometrical parameters of a stiffened FGM shell are given by: $k = 1; h = 0.01m; L = 3a; a = 100h$; $R = 400h$; the number of stiffeners: $n_1 = n_2 = 50$ (where n_1, n_2 are the number of stringer and rings of shell, respectively); $d_1 = d_2 = h/2$; $h_1 = h_2 = h/2$. Based on Eqs. (30) and (33), the post-buckling curves of a stiffened toroidal shell segment with various combinations of the mode (m, n, λ) are investigated. The corresponding curve to find the lower and upper critical loads is obtained. The lowest point of the curve is

Table 4 Lower critical load (GPa) with various modes (m, n, λ)

n	$m = 1$	$m = 2$	$m = 3$	$m = 4$
5	1.2734 (0.21)*	1.9226 (0.35)	2.0851 (0.31)	4.4533 (0.38)
6	1.1263 (0.32)	1.7276 (0.42)	1.8362 (0.42)	2.5217 (0.42)
7	**0.9953 (0.35)**	1.4043 (0.43)	1.3777 (0.48)	1.9697 (0.53)
8	1.0543 (0.46)	1.2808 (0.45)	1.7925 (0.59)	1.8310 (0.65)
9	1.1375 (0.61)	1.4504 (0.52)	2.2457 (0.67)	1.7183 (0.71)
10	1.1492 (0.75)	1.6455 (0.60)	2.2661 (0.70)	2.2710 (0.78)

* The number of λ

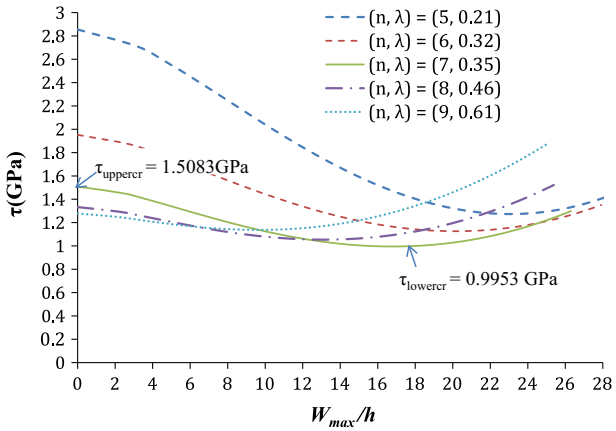

Fig. 2 Critical buckling load ($m = 1$)

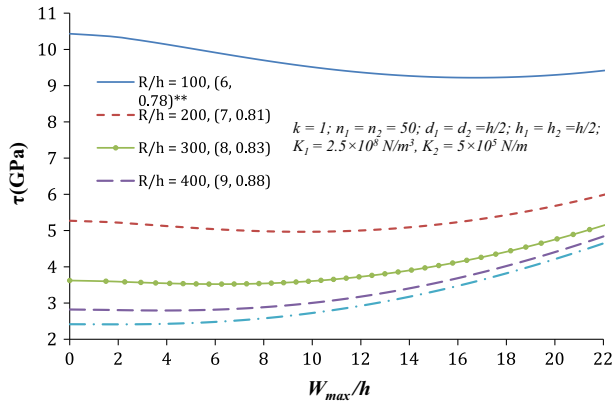

Fig. 3 Torsional post-buckling curves of a stiffened FGM convex shell on an elastic medium with effects of R/h ratio ($m = 1$, $h = 0.01m$, $L = 2a$, $a = 100h$). **Buckling mode (n, λ)

regarded as the critical condition. As can be seen from Table 1, the lower critical load is 0.9953 GPa with mode (1, 7, 0.35). Thus, the $\tau_{cr} \sim W_{max}/h$ curve in Fig. 2 describes the upper and lower critical loads at the $m = 1$ case. The linear critical load calculated by Eq. (31) $\tau_{linearcr} = 1.5083$ GPa with mode (1, 7, 0.35) completely coincides with the result of the upper critical buckling load in Fig. 2.

4.2.2 Effect of R/h ratio

The effect of the R/h on $\tau_{cr} \sim W_{max}/h$ post-buckling curves of a stiffened FGM convex and concave toroidal shell segment on an elastic medium ($K_1 = 2.5 \times 10^8$ N/m^3, $K_2 = 5 \times 10^5$ N/m) is illustrated in Figs. 3 and 4, respectively. It can be seen that the critical torsional buckling load τ_{cr} decreases when the R/h ratio increases for both stiffened FGM convex and concave toroidal shell segments (Table 4).

The torsional load carrying the more convex (concave) shells is higher than that of the less convex (concave) ones.

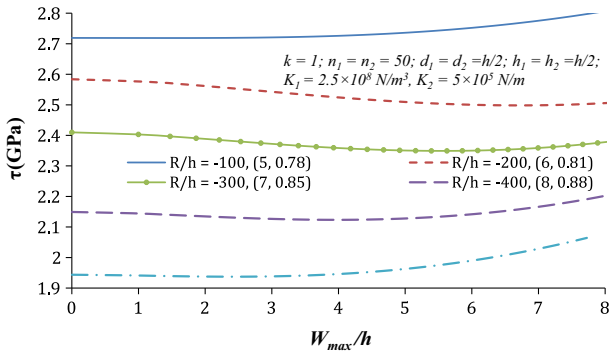

Fig. 4 Torsional post-buckling curves of a stiffened FGM concave shell on an elastic medium with effects of R/h ratio ($m = 1$, $h = 0.01m$, $L = 2a$, $a = 100h$)

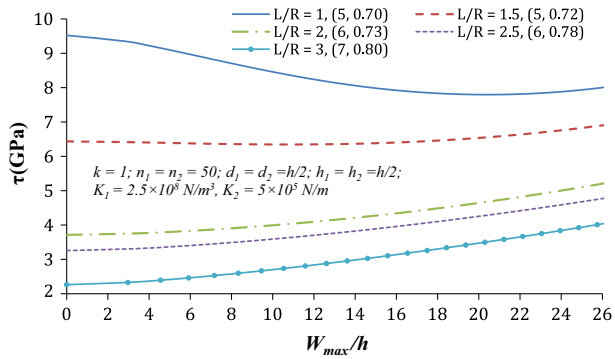

Fig. 5 Torsional post-buckling curves of a stiffened FGM concave shell on an elastic foundation with effects of L/R ratio ($m = 1$, $h = 0.01m$, $R = 200h$, $a = 100h$)

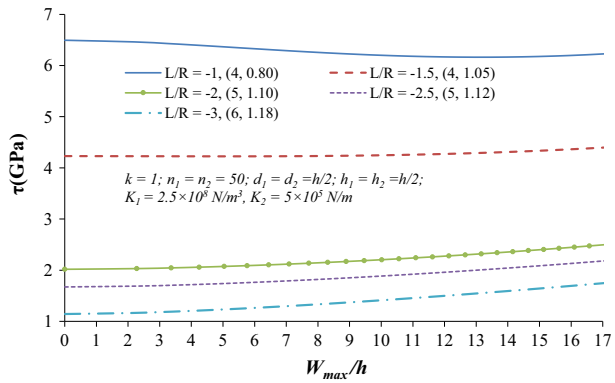

Fig. 6 Torsional post-buckling curves of a stiffened FGM concave shell on an elastic medium with effects of L/R ratio ($m = 1$, $h = 0.01m$, $R = 200h$, $a = 100h$)

4.2.3 Effect of L/R ratio

Similar to 4.2.2, effects of the L/R ratio on the torsional buckling load is investigated for both a stiffened FGM convex and concave shell on an elastic medium and represented in Figs. 5 and 6, respectively.

Based on Figs. 5 and 6, one can see that when the L/R ratio goes up, the critical torsional buckling loads decrease for both stiffened FGM convex and concave shells, but convex shells work better. The load carrying capacity of longer shells is lower than that of shorter ones. Particularly, from $L/R = 1$ to $L/R = 3$, the lower torsional load decreases about 70.99 % for a stiffened FGM convex shell and approximately 81.5 % for a stiffened FGM concave shell ().

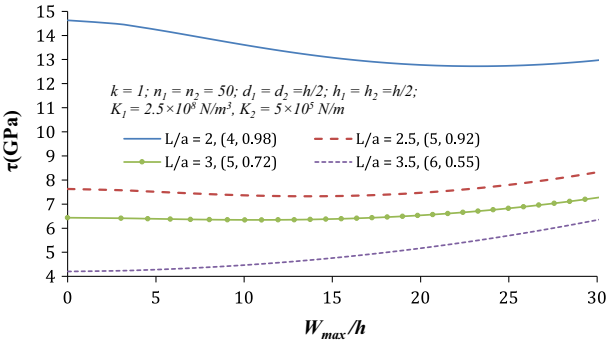

Fig. 7 Torsional post-buckling curves of a stiffened FGM convex shell on an elastic medium with effects of *L*/*a* ratio ($m = 1$, $h = 0.01m$, $a = 100h$, $R/h = 200$)

Table 5 Effect of mode and *L*/*a* ratio on the upper and lower critical loads (GPa; $m = 1$)

R/*h*	$L/a = 2$		$L/a = 2.5$		$L/a = 3$	
	Upper critical load calculated by Eq. (31)	Lower critical load calculated by Eqs. (30) and (33)	Upper critical load calculated by Eq. (31)	Lower critical load calculated by Eqs. (30) and (33)	Upper critical load calculated by Eq. (31)	Lower critical load calculated by Eqs. (30) and (33)
100	19.1886 (4, 1.10)	17.1865 (4, 1.10)	11.3422 (5, 0.88)	10.6674 (5, 0.88)	7.0943 (6, 0.85)	7.0666 (6, 0.85)
200	14.6288 (4, 0.98)	12.7234 (4, 0.98)	7.6285 (5, 0.92)	7.3263 (5, 0.92)	6.4354 (5, 0.72)	6.3449 (5, 0.72)
300	12.7829 (4, 0.86)	10.6615 (4, 0.86)	6.1497 (5, 0.65)	5.7704 (5, 0.65)	5.3847 (5, 0.82)	5.3556 (5, 0.82)
400	8.0186 (5, 0.88)	7.1926 (5, 0.88)	5.3320 (5, 0.58)	5.0458 (5, 0.58)	4.7929 (5, 0.75)	4.7757 (5, 0.75)

4.2.4 Effect of L/a ratio

The effect of *L*/*a* ratio on the torsional buckling load of a stiffened FGM convex shell on an elastic medium is also analyzed in Fig. 7.

It is observed that the critical torsional buckling load falls down when the *L*/*a* ratio increases. Table 5 presents the effect of *L*/*a* and *R*/*h* ratios with various modes (m, n, λ) on the critical loads ($a/h = 100$). The upper critical loads are calculated by Eq. (31), while the lower critical loads are computed by Eqs. (30) and (33).

As can be seen, the critical loads of the more convex shells are larger than those of the less convex ones, and the critical loads of shorter shells are larger than those of longer ones. For instance, when *L*/*a* ratio increases from 2 to 3 (*R*/*h* = 100), the lower torsional load falls down about 58.9 %, while the upper torsional load decreases by about 63 %. Moreover, for *R*/*h* = 400, the lower torsional load decreases about 34 % and the upper torsional load reduces to about 40 % when the *L*/*a* ratio goes up from 2 to 3.

4.2.5 Effect of volume fraction index

Figures 8 and 9 show the torsional buckling curves of stiffened FGM convex and concave shells on an elastic medium when the value of the volume fraction index changes from 0.5 to ∞. The geometrical parameters of the shell are: $a = 100h$; $h = 0.01m$; $L = 2a$; $d_1 = d_2 = h/2$; $h_1 = h_2 = h/2$; $n_1 = n_2 = 50$.

As can be seen, the torsional buckling curves falls down when the value volume fraction index increases for both stiffened FGM convex and concave shells.

Obviously, this property corresponds to the real characteristic of the material, because the higher value of k corresponds to a metal-richer shell which has less stiffness than a ceramic-richer one.

4.2.6 Comparison of torsional buckling loads of a stiffened and un-stiffened FGM toroidal shell segment

To investigate the effects of stiffeners, the database is used as:

$$m = 1;\ n = 5;\ \lambda = 0.90;\ h = 0.01m;\ a = 100h;\ L = 2a;\ R = 300h;\ K_1 = 2.5 \times 10^8\ \text{N/m}^3,$$
$$K_2 = 5 \times 10^5\text{N/m};\ d_1 = d_2 = h/2;\ h_1 = h_2 = h/2;\ n_1 = n_2 = 50.$$

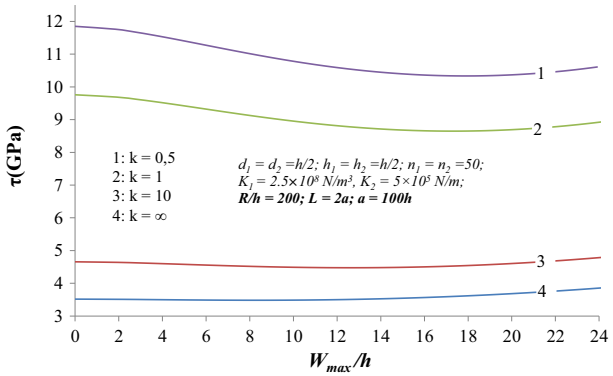

Fig. 8 Torsional post-buckling curves of a stiffened FGM convex shell on an elastic medium with effects of the volume fraction index ($m = 1, n = 5, \lambda = 0.88$)

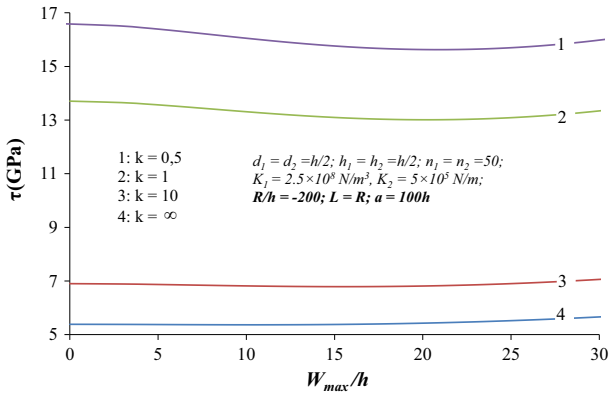

Fig. 9 Torsional post-buckling curves of a stiffened FGM convex shell on an elastic medium with effects of the volume fraction index ($m = 1, n = 3, \lambda = 0.95$)

Table 6 Torsional buckling loads of a stiffened and un-stiffened FGM toroidal shell segment (GPa)

Toroidal shell segment	$k = 0.5$	$k = 1$	$k = 5$	$k = 10$	$k = \infty$
Un-stiffened	9.1855	7.6869	4.6745	3.9702	3.0729
Stringer stiffened	9.1980	7.6989	4.6842	3.9795	3.0830
Ring stiffened	9.2307	7.7309	4.7186	4.0161	3.1247
Orthogonal stiffened	9.2434	7.7430	4.7288	4.0259	3.1354

As expected, the critical buckling loads of a stiffened FGM convex shell are larger than the corresponding values of an un-stiffened one. Moreover, the critical torsional buckling loads of an un-stiffened FGM convex shell are the smallest, the critical torsional loads of a ring stiffened FGM shell are higher than those of a stringer stiffened shell, and the critical torsional loads of stringer-ring stiffened ones are the largest. Thus, the stiffeners enhance the load carrying capacity of the shell (Table 6).

4.2.7 Effects of the number of stiffeners

The effects of the number of stiffeners are carried out with three categories: stringer stiffened, ring stiffened, and orthogonal stiffened. The geometric parameters are: $h = 0.01m;\ a = 100h;\ L = 3a;\ R = 200h;\ K_1 = 2.5 \times 10^8$ N/m^3, $K_2 = 5 \times 10^5$ N/m; $d_1 = d_2 = h/2;\ h_1 = h_2 = h/2$.

Based on Table 7, the critical torsional buckling load increases when the number of stiffeners goes up. Thus, the number of stiffeners makes the shells to become stiffer. If the number of stiffeners adds 10 stiffeners, the critical torsional load will increase from 0.01 to 0.08 % depending on the stiffener system. In addition, for the orthogonal stiffened system, the lower torsional load will increase about 0.34 % when the number of

Table 7 Effects of the number of stiffeners on the critical torsional buckling load (GPa; $m = 1$; $k = 1$)

Number of stiffeners	Stringer stiffened	Ring stiffened	Orthogonal stiffened
10	6.4167 (5, 0.55)	9.1936 (4, 0.68)	9.3415 (4, 0.98)
20	6.4195 (5, 0.55)	9.1964 (4, 0.68)	9.3493 (4, 0.98)
30	6.4224 (5, 0.55)	9.1991 (4, 0.68)	9.3572 (4, 0.98)
40	6.4252 (5, 0.55)	9.2019 (4, 0.68)	9.3650 (4, 0.98)
50	6.4281 (5, 0.55)	9.2046 (4, 0.68)	9.3728 (4, 0.98)
60	6.4309 (5, 0.55)	9.2074 (4, 0.68)	9.3806 (4, 0.98)
70	6.4337 (5, 0.55)	9.2101 (4, 0.68)	9.3883 (4, 0.98)
80	6.4365 (5, 0.55)	9.2128 (4, 0.68)	9.3961 (4, 0.98)
90	6.4393 (5, 0.55)	9.2155 (4, 0.68)	9.4038 (4, 0.98)
100	6.4422 (5, 0.55)	9.2182 (4, 0.68)	9.4115 (4, 0.98)

Table 8 Effects of the elastic medium on the critical torsional buckling load (GPa)

Elastic medium	Un-stiffened	Stringer stiffened	Ring stiffened	Orthogonal stiffened
$K_1 = 0;\ K_2 = 0.$	5.1470	5.1569	5.1658	5.1758
$K_1 = 2.5 \times 10^8$ N/m^3; $K_2 = 0.$	6.2529	6.2613	6.2733	6.2818
$K_1 = 2.5 \times 10^8$ N/m^3; $K_2 = 5 \times 10^5$ N/m.	6.3049	6.3133	6.3254	6.3338

stiffeners increases from 10 to 50 stiffeners and it increases about 0.75 % if the number of stiffeners goes up from 10 to 100 stiffeners.

4.2.8 Effects of the elastic medium

Table 8 illustrates the effects of the elastic medium on the critical torsional buckling load of an un-stiffened and stiffened FGM convex shell. The parameters of the shell are chosen: *a = 100h; L = 3a*; *R = 200h;* $m = 1$; $n = 5$; k = 1; $\lambda = 0.92$; $d_1 = d_2 = h/2$; $h_1 = h_2 = h/2$; $n_1 = n_2 = 50$.

It is observed that the critical torsional buckling loads of an FGM convex shell on a two-parameter elastic medium are the highest. For the shell without elastic medium, the critical torsional loads are lowest.

4.3 Results of nonlinear torsional buckling of internally stiffened FGM toroidal shell segments

The present results investigate the same toroidal shell segment which is made of FGM such that the inner side is metal rich and the internal metal stiffeners are put at this side. When the volume fraction index $k = 1$, it is available to compare the critical torsional buckling loads of both types of stiffened FGM toroidal shell segments.

4.3.1 Effects of R/h ratio

Firstly, the critical torsional buckling loads of an internally stiffened FGM toroidal shell segment with various *R/h* ratios are given in Tables 9 and 10, respectively. The geometric properties are similar to Sect. 4.2.2 and $k = 1$. Corresponding results for critical torsional loads of an externally stiffened FGM shell are taken from Figs. 3 and 4, respectively.

Based on both Tables 9 and 10, it can be seen that the critical torsional loads of an externally stiffened FGM shell are higher than those of an internally stiffened one.

Table 9 Critical torsional loads of a stiffened FGM convex toroidal shell segment with various *R/h* ratios (GPa)

R/h	Upper critical load		Lower critical load	
	Externally stiffened	Internally stiffened	Externally stiffened	Internally stiffened
100	10.4327 (6, 0.78)	10.3852 (6, 0.78)	9.2196 (6, 0.78)	9.1769 (6, 0.78)
200	5.2710 (7, 0.81)	5.2282 (7, 0.81)	4.9665 (7, 0.81)	4.9264 (7, 0.81)
300	3.6216 (8, 0.83)	3.5801 (8, 0.83)	3.5222 (8, 0.83)	3.4824 (8, 0.83)
400	2.8212 (9, 0.88)	2.7781 (9, 0.88)	2.7943 (9, 0.88)	2.7522 (9, 0.88)
500	2.4153 (10, 0.99)	2.3673 (10, 0.99)	2.4120 (10, 0.99)	2.3644 (10, 0.99)

Table 10 Critical torsional loads of a stiffened FGM concave toroidal shell segment with various *R*/*h* ratios (GPa)

R/*h*	Upper critical load		Lower critical load	
	Externally stiffened	Internally stiffened	Externally stiffened	Internally stiffened
−100	2.9544 (5, 0.78)	2.6948 (5, 0.78)	2.7187 (5, 0.78)	2.6946 (5, 0.78)
−200	2.5838 (6, 0.81)	2.5536 (6, 0.81)	2.4982 (6, 0.81)	2.4695 (6, 0.81)
−300	2.4099 (7, 0.85)	2.3760 (7, 0.85)	2.3492 (7, 0.85)	2.3167 (7, 0.85)
−400	2.2058 (8, 0.88)	2.1129 (8, 0.88)	2.1234 (8, 0.88)	2.0882 (8, 0.88)
−500	2.0643 (9, 0.92)	1.9047 (9, 0.92)	1.9373 (9, 0.92)	1.8988 (9, 0.92)

Table 11 Critical torsional loads of a stiffened FGM toroidal shell segment with various stiffeners (GPa)

Toroidal shell segment	Externally stiffened	Internally stiffened
Stringer stiffened	7.6989	7.6908
Ring stiffened	7.7309	7.6978
Orthogonal stiffened	7.7430	7.7018

Table 12 Critical torsional loads of a stiffened FGM toroidal shell segment on an elastic medium (GPa)

Shell	$K_1 = 0;\ K_2 = 0$	$K_1 = 2.5 \times 10^8$ N/m^3; $K_2 = 0$	$K_1 = 2.5 \times 10^8$ N/m^3; $K_2 = 5 \times 10^5$ N/m
Stringer stiffened			
Externally stiffened	5.1569	6.2613	6.3133
Internally stiffened	5.1503	6.2543	6.3065
Ring stiffened			
Externally stiffened	5.1658	6.2733	6.3254
Internally stiffened	5.1504	6.2570	6.3090
Orthogonal stiffened			
Externally stiffened	5.1758	6.2818	6.3338
Internally stiffened	5.1538	6.2583	6.3104

4.3.2 Comparison of critical loads of an internally and externally stiffened FGM toroidal shell segment with various stiffeners

Secondly, the critical torsional loads of various stiffened FGM shells are given in Table 11 to compare between externally stiffened FGM and internally stiffened FGM shells. The parameters here are similar to Sect. 4.2.6 and $k = 1$. As can be seen, the critical torsional loads of an externally stiffened FGM shell are higher than those of internally stiffened in three stiffener categories. Also, for an internally stiffened FGM shell, the critical torsional buckling loads of a ring stiffened FGM shell are higher than those of a stringer one.

4.3.3 Effects of the elastic medium

Finally, Table 12 illustrates the critical torsional load of a stiffened FGM toroidal shell on an elastic medium. The database used is similar to Sect. 4.2.8. Corresponding critical torsional loads of externally stiffened shells are taken from Table 8.

It is regarded that the critical torsional loads of an externally stiffened FGM shell are higher than those of an internally stiffened one. Furthermore, the critical torsional loads on a Pasternak elastic medium are the highest, while those without an elastic medium are the smallest.

5 Conclusions

An analytical approach to analyze the torsional buckling and post-buckling behavior of an eccentrically stiffened FGM toroidal shell segment based on the classical shell theory and the smeared stiffeners technique with geometrical nonlinearity in von Kármán sense is investigated. The results are shown:

– The deflection of the shell is more correctly expressed in the form of three-term equation including the linear and nonlinear buckling shape.

– The closed-form expressions to find the critical torsional load and post-buckling load-deflection curves are obtained.
– The stiffener system is used to enhance strongly the stability and the load carrying capacity of an FGM toroidal shell segment.
– Effects of geometric parameters, volume fraction index, various stiffeners, number of stiffeners, and elastic medium are investigated.
– The present result shows that the critical torsional loads of an externally stiffened FGM toroidal shell segment are higher than those of an internally stiffened one. Thus, the toroidal shell segment with externally stiffened FGM is better used and more preeminent.

Acknowledgments This research is funded by the Vietnam National Foundation for Science and Technology Development (NAFOSTED) under Grant Number 107.02-2014.09.

References

1. Koizumi, M.: The concept of FGM, ceramic transactions. Funct. Grad. Mater. **34**, 3–10 (1993)
2. Sofiyev, A.H., Kuruoglu, N.: Torsional vibration and buckling of the cylindrical shell with functionally graded coatings surrounded by an elastic medium. Compos. Part B **45**, 1133–1142 (2013)
3. Najafov, A.M., Sofiyev, A.H., Kuruoglu, N.: Torsional vibration and stability of functionally graded orthotropic cylindrical shells on elastic foundation. Meccanica **48**, 829–840 (2013)
4. Batra, R.C.: Torsion of a functionally graded cylinder. AIAA J. **44**, 1363–1365 (2006)
5. Shen, H.S.: Torsional buckling and postbuckling of FGM cylindrical shells in thermal environments. Int. J. Non-Linear Mech. **44**, 644–657 (2009)
6. Sofiyev, A.H., Schnack, E.: The stability of functionally graded cylindrical shells under linearly increasing dynamic torsional loading. Eng. Struct. **26**, 1321–1331 (2004)
7. Huang, H., Han, Q.: Nonlinear buckling of torsion-loaded functionally graded cylindrical shells in thermal environment. Eur. J. Mech. A Solids **29**, 42–48 (2010)
8. Wang, H.M., Liu, C.B., Ding, H.J.: Exact solution and transient behavior for torsional vibration of functionally graded finite hollow cylinders. Acta Mech. Sin. **25**, 555–563 (2009)
9. Arghavan, S., Hematiyan, M.R.: Torsion of functionally graded hollow tubes. Eur. J. Mech. A Solids **28**, 551–559 (2009)
10. Tan, D.: Torsional buckling analysis of thin and thick shells of revolution. Int. J. Solids Struct. **37**, 3055–3078 (2000)
11. Dung, D.V., Hoa, L.K.: Research on nonlinear torsional buckling and post-buckling of eccentrically stiffened functionally graded thin circular cylindrical shells. Compos. Part B **51**, 300–309 (2013)
12. Sofiyev, A.H., Adiguzel, S.S.: Torsional stability of cylindrical shells with functionally graded middle layer on the Winkler elastic foundation. J. Solid Mech. **3**, 218–227 (2011)
13. Zhang, P., Fu, Y.: Torsional buckling of elastic cylinders with hard coatings. Acta Mech. **220**, 275–287 (2011)
14. Dung, D.V., Hoa, L.K.: Nonlinear torsional buckling and post-buckling of eccentrically stiffened FGM cylindrical shells in thermal environment. Compos. Part B **69**, 378–388 (2015)
15. Huang, H., Han, Q.: Nonlinear buckling and postbuckling of heated functionally graded cylindrical shells under combined axial compression and radial pressure. Int. J. Non-Linear Mech. **44**, 209–218 (2009)
16. Bich, D.H., Phuong, N.T., Tung, H.V.: Buckling of functionally graded conical panels under mechanical loads. Compos. Struct. **91**, 1379–1384 (2012)
17. Sofiyev, A.H.: Non-linear buckling behavior of FGM truncated conical shells subjected to axial load. Int. J. Non-Linear Mech. **46**, 711–719 (2011)
18. Duc, N.D., Quan, T.Q.: Nonlinear postbuckling of imperfect eccentrically stiffened P-FGM double curved thin shallow shells on elastic foundations in thermal environments. Compos. Struct. **106**, 590–600 (2013)
19. Duc, N.D., Thang, P.T.: Nonlinear response of imperfect eccentrically stiffened ceramic–metal–ceramic FGM thin circular cylindrical shells surrounded on elastic foundations and subjected to axial compression. Compos. Struct. **110**, 200–206 (2014)
20. Shen, H.S.: Postbuckling analysis of axially-loaded functionally graded cylindrical shells in thermal environments. Compos. Sci. Technol. **62**, 977–987 (2002)
21. Shariyat, M.: Dynamic buckling of suddenly loaded imperfect hybrid FGM cylindrical shells with temperature-dependent material properties under thermo-electro-mechanical loads. Int. J. Mech. Sci. **50**, 1561–1571 (2008)
22. Liew, K.M.: Postbuckling responses of functionally graded cylindrical shells under axial compression and thermal loads. Compos. Part B **43**, 1621–1630 (2012)
23. Kadoli, R., Ganesan, N.: Buckling and free vibration analysis of functionally graded cylindrical shells subjected to a temperature-specified boundary condition. J. Sound Vib. **289**, 450–480 (2006)
24. Huang, H., Han, Q., Wei, D.: Buckling of FGM cylindrical shells subjected to pure bending load. Compos. Struct. **93**, 2945–2952 (2011)
25. Sofiyev, A.H., Kuruoglu, N., Turkmen, M.: Buckling of FGM hybrid truncated conical shells subjected to hydrostatic pressure. Thin-Walled Struct. **47**, 61–72 (2009)
26. Zenkour, A.M., Sobhy, M.: Thermal buckling of various types of FGM sandwich plates. Compos. Struct. **93**, 93–102 (2010)
27. Winkler, E.: Die Lehre von der Elasticitaet und Festigkeit. Dominicus, Prague (1867)
28. Pasternak, P.L.: On a new method of analysis of an elastic foundation by means of two foundation constants. Gos. Izd. Lit. po strait i Arkh, Moscow, Russia; 1954 (In Russian)

29. Bagherizadeh, E., Kiani, Y., Eslami, M.R.: Mechanical buckling of functionally graded material cylindrical shells surrounded by Pasternak elastic foundation. Compos. Struct. **93**, 3063–3071 (2011)
30. Shen, H.S.: Postbuckling of shear deformable FGM cylindrical shells surrounded by an elastic medium. Int. J. Mech. Sci. **51**, 372–383 (2009)
31. Shen, H.S.: Postbuckling of internal pressure loaded FGM cylindrical shells surrounded by an elastic medium. Eur. J. Mech. A Solids **29**, 448–460 (2010)
32. Sofiyev, A.H.: Buckling analysis of FGM circular shells under combined loads and resting on the Pasternak type elastic foundation. Mech. Res. Commun. **37**, 539–544 (2010)
33. Sofiyev, A.H.: Thermal buckling of FGM shells resting on a two-parameter elastic foundation. Thin-Walled Struct. **49**, 1304–1311 (2011)
34. Sofiyev, A.H.: The effect of elastic foundations on the nonlinear buckling behavior of axially compressed heterogeneous orthotropic truncated conical shells. Thin-Walled Struct. **80**, 178–191 (2014)
35. Sofiyev, A.H., Kuruoglu, N.: Non-linear buckling of an FGM truncated conical shell surrounded by an elastic medium. Int. J. Press. Vessels Pip. **107**, 38–49 (2013)
36. Stein, M., McElman, J. A.: Buckling of segments of toroidal shells. AIAA J. **3**, 1704–1709 (1965)
37. Hutchinson John, W.: Initial post-buckling behavior of toroidal shell segments. J. Solid Struct. **3**, 97–115 (1967)
38. Parnell, T.K.: Numerical improvement of asymptotic solution for shells of revolution with application to toroidal shell segments. Comput. Struct. **16**, 109–117 (1983)
39. Brush, D.O., Almorth, B.O.: Buckling of Bars, Plates and Shells. Mc Graw-Hill, New York (1975)
40. Nash, W.A.: An experimental analysis of the buckling of thin initially imperfect cylindrical shells subject to torsion. Proc. Soc. Exp. Stress Anal. **16**, 55–68 (1959)
41. Ekstrom, R.E.: Buckling of cylindrical shells under combined torsion and hydrostatic pressure. Exp. Mech. **3**, 192–197 (1963)